Discovery of an Accreting Millisecond Pulsar in the Eclipsing Binary System SWIFT J1749.4-2807

Altamirano, D.; Cavecchi, Y.; Patruno, A.; Watts, A.; Linares, M.; Degenaar, N.; Kalamkar, M.; van der Klis, M.; Rea, N.; Casella, P.

Published in:
Astrophysical Journal Letters

DOI:
10.1088/2041-8205/727/1/L18

The Astrophysical Journal Letters, 727:L18 (5pp), 2011 January 20 doi:10.1088/2041-8205/727/1/L18

DISCOVERY OF AN ACCRETING MILLISECOND PULSAR IN THE ECLIPSING BINARY SYSTEM SWIFT J1749.4–2807

D. Altamirano[1], Y. Cavecchi[1,2], A. Patruno[1], A. Watts[1], M. Linares[3], N. Degenaar[1], M. Kalamkar[1], M. van der Klis[1], N. Rea[4], P. Casella[5], M. Armas Padilla[1], R. Kaur[1], Y. J. Yang[1], P. Soleri[6], and R. Wijnands[1]
[1] Astronomical Institute, "Anton Pannekoek," University of Amsterdam, Science Park 904, 1098XH, Amsterdam, The Netherlands; d.altamirano@uva.nl
[2] Sterrewacht Leiden, University of Leiden (Huygens Laboratory J. H. Oort Building), Niels Bohrweg 2, NL-2333 CA Leiden, The Netherlands
[3] Massachusetts Institute of Technology–Kavli Institute for Astrophysics and Space Research, Cambridge, MA 02139, USA
[4] Institut de Ciencies de l'Espai (ICE, CSIC–IEEC), Campus UAB, Facultat de Ciencies, Torre C5-parell, 2a planta, 08193, Bellaterra (Barcelona), Spain
[5] School of Physics and Astronomy, University of Southampton, Southampton, Hampshire SO17 1BJ, UK
[6] Kapteyn Astronomical Institute, University of Groningen, P.O. Box 800, 9700 AV Groningen, The Netherlands
Received 2010 May 19; accepted 2010 December 9; published 2010 December 28

ABSTRACT

We report on the discovery and the timing analysis of the first eclipsing accretion-powered millisecond X-ray pulsar (AMXP): SWIFT J1749.4–2807. The neutron star rotates at a frequency of ∼517.9 Hz and is in a binary system with an orbital period of 8.8 hr and a projected semimajor axis of ∼1.90 lt-s. Assuming a neutron star between 0.8 and 2.2 $M_{\odot}$ and using the mass function of the system and the eclipse half-angle, we constrain the mass of the companion and the inclination of the system to be in the ∼0.46–0.81 $M_{\odot}$ and ∼ 74.°4–77.°3 range, respectively. To date, this is the tightest constraint on the orbital inclination of any AMXP. As in other AMXPs, the pulse profile shows harmonic content up to the third overtone. However, this is the first AMXP to show a first overtone with rms amplitudes between ∼6% and ∼23%, which is the strongest ever seen and which can be more than two times stronger than the fundamental. The fact that SWIFT J1749.4–2807 is an eclipsing system that shows uncommonly strong harmonic content suggests that it might be the best source to date to set constraints on neutron star properties including compactness and geometry.

Key words: pulsars: general – pulsars: individual (SWIFT J1749.4–2807) – stars: neutron

Online-only material: color figures

1. INTRODUCTION

The first accreting millisecond X-ray pulsar (hereafter AMXP) was discovered in 1998 (SAX J1808.4–3658; see Wijnands & van der Klis 1998) and since then, a total of 13 AMXPs have been found and studied in detail (Patruno 2010). Most AMXPs show near sinusoidal profiles during most of their outbursts. This is consistent with a picture in which only one of the hot spots (at the magnetic poles) is visible (see references below). Deviations from a sinusoidal profile (i.e., an increase in harmonic content) are generally interpreted as being caused by the antipodal spot becoming visible, perhaps as accretion rate falls and the disk retreats (see, e.g., Poutanen & Gierliński 2003; Ibragimov & Poutanen 2009, and references therein).

Although the amplitude of the first overtone may reach that of the fundamental late in the outburst (see, e.g., Hartman et al. 2008, 2009), no AMXP so far has shown pulse profiles where the first overtone is generally stronger than the fundamental throughout the outburst.

The stability of the pulse profiles in some of the AMXPs means that pulse-profile modeling can be used to set bounds on the compactness of the neutron star and hence the dense matter equation of state (EoS; see, e.g., Poutanen & Gierliński 2003; Poutanen et al. 2009, and references therein). Unfortunately, there is often a large degeneracy between the parameters due to the number of free parameters needed to construct the model profile. One of these parameters is the inclination of the system, which to date has not been well constrained for any AMXP.

In this Letter, we report on the discovery and timing of the AMXP SWIFT J1749.4–2807. Thanks to the observed eclipses (Markwardt et al. 2010), we set the tightest constraint on system inclination for any AMXP. This, coupled with the fact that the amplitude of the first overtone is higher/comparable to that of the fundamental for much of the outburst and that the amplitude of the first overtone is unusually high, allows to put tight constraints on pulse-profile models. We show that SWIFT J1749.4–2807 has the potential to be one of the best sources for this approach to constraining the neutron star mass–radius relation and hence the EoS of dense matter.

2. SWIFT J1749.4–2807

SWIFT J1749.4–2807 was discovered in 2006 June 2 (Schady et al. 2006), when a bright burst was detected by the *Swift* burst alert telescope (BAT). Wijnands et al. (2009) presented a detailed analysis of the *Swift*/BAT and *Swift*/XRT data and showed that the spectrum of the 2006 burst was consistent with that of a thermonuclear Type I X-ray burst (see also Palmer et al. 2006; Beardmore et al. 2006) from a source at a distance of 6.7 ± 1.3 kpc.

SWIFT J1749.4–2807 was detected again between 2010 April 10 and 13 using *INTEGRAL* and *Swift* observations (Pavan et al. 2010; Chenevez et al. 2010). We promptly triggered approved *Rossi X-ray Timing Explorer* (*RXTE*) observations on this source to study X-ray bursts and to search for millisecond pulsations (Proposal ID:93085-09, PI: Wijnands). The first *RXTE* observation was performed on April 14 and lasted for about 1.6 ks. We found strong coherent pulsations at ≈517.9 Hz and at its first overtone ≈1035.8 Hz, showing that SWIFT J1749.4–2807 is an accreting millisecond X-ray pulsar (Altamirano et al. 2010). *RXTE* followed up the decay of the outburst on a daily basis. Preliminary results on the rms amplitude of the pulsations, orbital solution, discovery

of eclipses, evolution of the outburst, and upper limits on the quiescent luminosity were reported in Astronomer's Telegrams (Altamirano et al. 2010; Bozzo et al. 2010; Belloni et al. 2010; Strohmayer & Markwardt 2010; Markwardt et al. 2010; Yang et al. 2010; Chakrabarty et al. 2010). No optical counterpart has been identified as yet, with a 3σ lower limit in the *i* band of 19.6 (Yang et al. 2010).

3. OBSERVATIONS, SPECTRAL ANALYSIS, AND BACKGROUND ESTIMATION

We used data from the *RXTE* Proportional Counter Array (PCA; for instrument information see Jahoda et al. 2006). Between April 14 and April 21 there were 15 pointed observations of SWIFT J1749.4–2807, each covering 1 or 2 consecutive 90 minute satellite orbits.

We also analyzed data from *Swift*'s X-ray telescope (XRT; Burrows et al. 2005). There were a total of 10 observations (target ID 31686), all obtained in the Photon Counting (PC) mode.

We used standard tools and procedures to extract energy spectra from PCA Standard 2 data. We calculated response matrices and ancillary files for each observation using the `FTOOLS` routine `PCARSP V10.1`. Background spectra were estimated using the faint model in `PCABACKEST` (version 6.0). For the XRT, we used standard procedures to process and analyze the PC mode data.[7] When necessary, an annular extraction region was used to correct for pileup effects. We generated exposure maps with the task `XRTEXPOMAP`, and ancillary response files were created with `XRTMKARF`. The latest response matrix files (v. 11) were obtained from the `CALDB` database.

We used an absorbed power law to fit all PCA/XRT observations. We first fitted all XRT spectra and found an average interstellar absorption of 3.5×10^{22} cm^{-2}; N_H was fixed to this value when fitting all (standard) background-subtracted PCA spectra. When comparing the fluxes estimated by PCA and XRT we found that the PCA fluxes were systematically higher. Only on one occasion *RXTE* and *Swift* observations were performed simultaneously (MJD 55306.69, i.e., at the end of the outburst) and in this case the flux difference was $\approx 1.4 \times 10^{-10}$ erg cm^{-2} s^{-1}. This is consistent with that seen a day later. Since (1) the count rates during the last *RXTE* observation (when the source was below the PCA detection limit but detected by *Swift*/XRT) are consistent with those we measure during the eclipses (see Section 6) and (2) these count rates are consistent with the offset we find between PCA and XRT, we conclude that there is an additional source of background flux in our PCA observations. To correct for this, we also use the background-corrected spectrum of the last PCA observation (ObsID: 95085-09-02-08, MJD 55307.5) as an estimate of the additional source of background flux. This approach is optimal in crowded fields near the Galactic plane, where the contribution from the Galactic ridge emission and other X-ray sources in the 1° PCA field of view becomes important (see, e.g., Linares et al. 2007, 2008).

3.1. Background Estimates and the Fractional rms Amplitudes

Given the low flux during our observations, it is very important to accurately estimate the background emission before calculating the pulse fractional rms amplitudes. The fact that the extra source of background photons is unknown complicates the estimation of total background flux as a function of time. For example, the background flux could be intrinsically varying; even in the case of a constant distribution of background flux in the sky, it would be possible to measure flux variations if the collimator (i.e., PCA) orientation on the sky changes between observations. Given the background uncertainties, we arbitrarily adopt as total 3–16 keV background per observation the modeled background plus a constant offset of $\approx 17.5 \pm 2$ counts s^{-1} PCU^{-1}. This takes into account the $\approx$19.5 counts s^{-1} PCU^{-1} as estimated by the eclipses, the last PCA observation, and the PCA−XRT offset (which is equivalent to $\approx$18–19 counts s^{-1} PCU^{-1} in the 3–16 keV band as estimated with WebPIMMS[8] and the best-fit model to the XRT data), and the $\approx$15.5 offset we would obtain if the additional source of background photons could change by $\sim$20%. This conservative adopted possible background range results in conservative errors on the pulsed fractions we report, i.e., the errors are probably overestimated.

4. OUTBURST EVOLUTION

In Figure 1, we show the 2.0–10.0 keV unabsorbed flux of SWIFT J1749.4–2807 as measured from all available *RXTE*/PCA and *Swift*/XRT observations. Our data set samples the last seven days of the outburst, during which the flux decayed exponentially. We find that between MJD 55306.5 and 55307.5 SWIFT J1749.4–2807 underwent a sudden drop in flux of more than an order of magnitude, less abrupt than the three orders of magnitude drop in flux observed in the previous outburst of SWIFT J1749.4–2807 (Wijnands et al. 2009). Similar drops in flux have been seen for other AMXPs (see, e.g., Wijnands et al. 2003; Patruno et al. 2009b). If we take into account the fact that SWIFT J1749.4–2807 was first detected on MJD 55296 (Pavan et al. 2010), we estimate an outburst duration of about 12 days.

5. PULSATIONS

Adopting a source position $\alpha = 17^{\rm h}49^{\rm m}31\overset{\rm s}{.}94$, $\delta = -28°08'05\overset{''}{.}8$ (from *XMM-Newton* images, see Wijnands et al. 2009), we converted the photon arrival times to the solar system barycenter (Barycentric Dynamical Time) with the FTOOL faxbary, which uses the JPL DE-405 ephemeris along with the spacecraft ephemeris and fine clock corrections to provide an absolute timing accuracy of 3.4 μs (Jahoda et al. 2006).

We created power spectra of segments of 512 s of data and found strong signals at frequencies of $\approx$517.92 Hz and $\approx$1035.84 Hz (Altamirano et al. 2010); these signals were not always detected simultaneously with a significance greater than 3σ.

To proceed further, we used the preliminary orbital solution reported by Strohmayer & Markwardt (2010) and folded our data set into 87 pulse profiles of $\approx$500 s each. We then fitted the profiles with a constant plus four sinusoids representing the pulse frequency and its overtones. We then phase connected the pulse phases by fitting a constant pulse frequency plus a circular Keplerian orbital model. The procedure is described in detail in Patruno et al. (2010). In Table 1, we report the best-fit solution and in Figure 2 we show one example of the pulse profile.

It is known that the timing residuals represent a significant contribution to the X-ray timing noise, which if not properly taken into account can affect the determination of the pulse

[7] http://www.swift.ac.uk/XRT.shtml

[8] http://heasarc.gsfc.nasa.gov/Tools/w3pimms.html

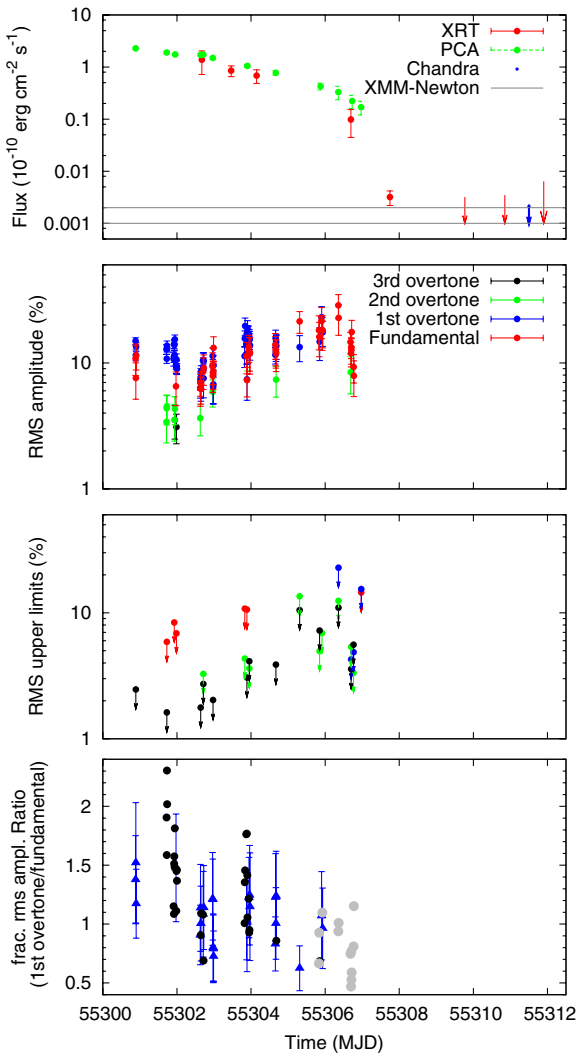

Figure 1. Top panel: 2–10 keV flux as measured from *RXTE*/PCA and *Swift*/XRT observations. The flux of the last PCA observation (MJD 55307.5) is not shown; the spectrum of this observation was used as an estimate background emission (see the text). Upper limits are quoted at 95% confidence level. We calculated the flux during the last PCA and last *Swift*/XRT detection using WebPIMMS (assuming a power-law spectrum with index 1.8). Middle panels: fractional rms amplitude and 95% confidence level upper limits of the fundamental and three overtones as a function of time. Detections ($>3\sigma$ single trial) and upper limits are from ∼500 and ∼3000 s data sets, respectively. Bottom panel: ratio between the fractional rms amplitude of the first overtone and fundamental. Blue triangles represent points in which both harmonics are significantly detected in ≈500 s data sets. Black circles represent the ratio between the fractional rms amplitude of the first overtone and the 95% confidence level upper limit to the amplitude of the fundamental. Gray circles represent the same ratio but when the fundamental is significantly detected and not the first overtone. This means that black circles represent lower limits while gray circles are upper limits. These ratios are independent of the background.

(A color version of this figure is available in the online journal.)

frequency and the orbital solution (see, e.g., Hartman et al. 2008; Patruno et al. 2010). There is a hint of a correlation between the X-ray timing noise and the X-ray flux, especially between MJD 55302 and 55303, where a slight increase of the X-ray flux is accompanied by a jump in the pulse phases, similarly to what was reported for six other AMXPs by Patruno et al. (2009a). A complete discussion of timing noise in this source is beyond the scope of this Letter and will be presented elsewhere.

In the middle panels of Figure 1 we show the fractional rms amplitude of the fundamental, and of the first, second, and third

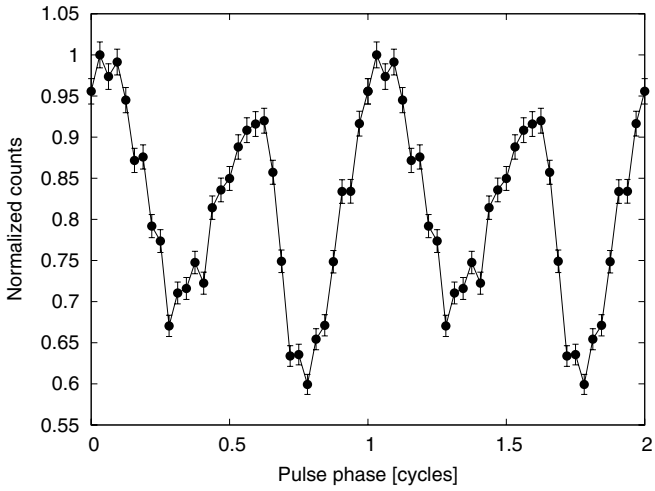

Figure 2. Pulse profile obtained by folding ≈3400 s of data (ObsID: 95085-09-01-02, 2–16 keV range).

Table 1
Timing Parameters for the AMXP SWIFT J1749.4–2807

Parameter	Value
Orbital period, $P_{\rm orb}$(days)	0.3673696(2)
Projected semimajor axis, $a_x \sin i$ (lt-s)	1.89953(2)
Time of ascending node, $T_{\rm asc}$ (MJD) .	55300.6522536(7)
Eccentricity, e (95% c.l.)	$< 5.2 \times 10^{-5}$
Spin frequency ν_0 (Hz)	517.92001395(1)
Pulsar mass function, f_x ($M_\odot$)	0.0545278(13)
Minimum companion mass[a], M_c ($M_\odot$)	0.5898

Notes. All errors are at $\Delta\chi^2 = 1$.
[a] The companion mass is estimated assuming a neutron star of 1.4 $M_\odot$.

overtones when the signal was $>3\sigma$ significant in ∼500 s data sets. The 95% confidence level upper limits are estimated using ∼3000 s data sets (excluding detections) and plotted separately for clarity. When detected significantly, the rms amplitudes of the fundamental and the first overtone are in the ≃6%–29% and ≃6%–23% ranges, respectively; the highest values are reached at the end of the outburst, where the uncertainties in our measurements also increase. Amplitudes for the fundamental as high as 15%–20% rms have been seen before for at least one source (although for a brief interval; see Patruno et al. 2010), however, no other AMXP shows a first overtone as strong as we detect it in SWIFT J1749.4–2807. In order to compare the strength of both signals, in Figure 1 (lower panel) we show the ratio between the fractional rms amplitude of the first overtone and that of the fundamental. As can be seen, there are periods in which the ratio is approximately 1, but also periods where the ratio is 2 or more. We note that these ratios are independent of the uncertainties on the background.

6. ECLIPSES AND THE INCLINATION OF THE SYSTEM

We searched the *RXTE* data for the occurrence of X-ray bursts and found none. Following Markwardt et al. (2010), we also searched for possible signatures of eclipses and found two clear cases in the *RXTE* data (ObsIDs: 95085-09-02-02 and 95085-09-02-04, beginning at MJD 55302.97 and 55305.87, respectively). PCA data on MJD 55306.97 (ObsID: 95089-09-02-11) sample an ingress, however, the count rate is too low to extract useful information (but see Markwardt & Strohmayer 2010; Ferrigno et al. 2011).

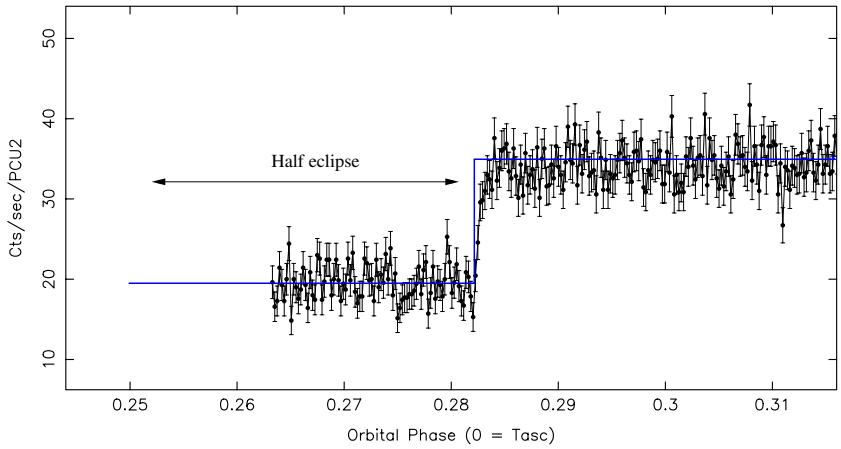

Figure 3. Eclipse observed on observation 95085-09-02-02. The data set starts on MJD 55302.9531, during the eclipse and shows that the egress occurs at orbital phase ≈0.282 (where orbital phase zero is the time of passage through the ascending node). We estimate the duration of the eclipse by assuming that eclipse is symmetric around orbital phase 0.25. The light curve was only corrected by the standard modeled background (see the text). Count rates are in the 2–16 keV band.
(A color version of this figure is available in the online journal.)

The first and clearest case of an eclipse is shown in Figure 3. The average 3–16 keV count rate at the beginning of the observation is about ≈18.5–19.5 counts s^{-1} $PCU2^{-1}$ (only the standard modeled background has been subtracted) for the first ≈600 s. Then the count rate increases within a few seconds to an average of ≈36 counts s^{-1} $PCU2^{-1}$ and remains approximately constant for the rest of the data set. The other data set also shows a similar low-to-high count rate transition although at lower intensities: the observation samples less than 275 s of the eclipse (at a rate of ≈18–19 counts s^{-1} $PCU2^{-1}$); the count rate after the egress is about ≈22 counts s^{-1} $PCU2^{-1}$, i.e., much lower than in the previous case.

Within the uncertainties on the unmodeled background, both egresses occur between orbital phases of ≈0.2823–0.2825. During the eclipse the count rates in these two observations are consistent with the expected background of ≈18–19 counts s^{-1} $PCU2^{-1}$, implying that that SWIFT J1749.4–2807 most probably shows total eclipses; however, given the uncertainties in the background (see Section 3.1) and the sensitivity of the PCA, this should be tested and better quantified with observations from instruments like *XMM-Newton*, *Suzaku*, or *Chandra* (see also Pavan et al. 2010; Ferrigno et al. 2011).

Using the best solution reported in Table 1, we also searched for pulsations in the 600 s period during which the companion star is eclipsing the neutron star (see above). We found none. Upper limits are unconstrained.

With our improved orbital solution and the measured times of the two egresses, we determine the phase of egress to be no larger than 0.2825. Assuming that the eclipses are centered around neutron star superior conjunction, the eclipse half-angle is ≈11.°7, corresponding to an eclipse duration of ≈2065 s.

We do not detect any evidence of absorption in the form of dips in the light curves, probably due to the fact that our data set only samples ≈1.5 orbital periods. These dips are common in other eclipsing LMXBs and thought to be due to the interaction of the photons from the central X-ray emitting region by structure on the disk rim or by what is left of the stream of incoming matter (from the companion) above and below the accretion disk. These dips are known to be highly energy dependent; both eclipses and egresses in our data are energy independent.

Assuming that the companion star is a sphere with a radius R equal to the mean Roche lobe radius, then the radius of the companion star can be approximated as

$$R_L = a \cdot \frac{0.49 \cdot q^{2/3}}{0.6 \cdot q^{2/3} + \ln(1 + q^{1/3})}, \quad (1)$$

where a is the semimajor axis of the system and $q = M_c/M_{\rm NS}$ is the ratio between the companion and neutron star masses, respectively (Eggleton 1983). From geometrical considerations in an eclipsing system, if the size of the X-ray emitting region is negligible compared with the radius of the companion star, then R_L is also related to the inclination i and the eclipse half-angle ϕ:

$$R_L = a \cdot \sqrt{\cos^2 i + \sin^2 i \cdot \sin^2 \phi}, \quad (2)$$

when the eccentricity of the system is zero (see, e.g., Chakrabarty et al. 1993; also note that the half-angle of the eclipse might be smaller as the star filling its Roche lobe is not spherical, see, e.g., Chanan et al. 1976). These two equations in combination with the mass function form a system of equations that allow us to find the inclination of the binary system as a function of the neutron star and companion star mass. In Figure 4, we show our results. For a neutron star with mass in the 0.8–2.2 (1.4–2.2) $M_\odot$ range, we find inclinations in the 74.°4–77.°3 (76.°3–77.°3) range and companion mass in the 0.46–0.81 (0.67–0.81) $M_\odot$ range.

7. CONSTRAINING NEUTRON STAR PROPERTIES VIA PULSE-PROFILE MODELING

Knowing the inclination to a high degree of precision is useful for pulse-profile modeling to constrain neutron star properties including compactness and geometry. To explore what could be done, we tried fitting simple model light curves to the pulse amplitude observations (along the lines explored by Pechenick et al. 1983, Nath et al. 2002, and Cadeau et al. 2007). The code we use has been tested against, and is in good agreement with, the results of Lamb et al. (2009).

We assume isotropic blackbody emission from one or two antipodal circular hot spots, and no emission from the rest of the star or the disk. At this stage we ignore both Comptonization (which might be important; Gierliński & Poutanen 2005) and disk obscuration.

We consider as free parameters stellar mass and radius, and the colatitude α and angular half-size δ of the hot spot(s). Using

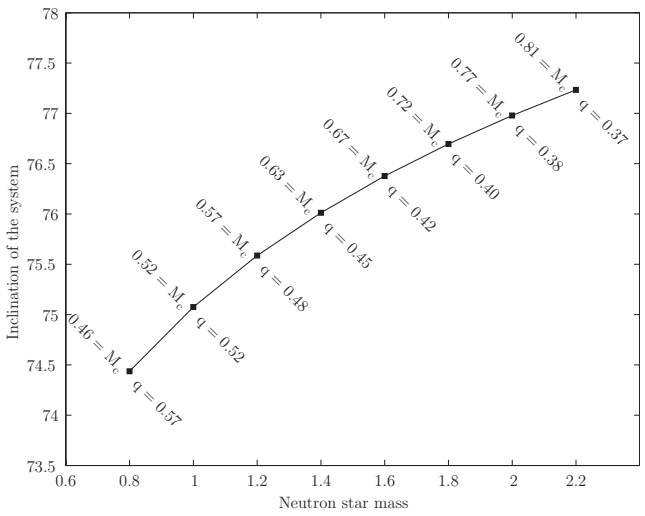

Figure 4. Inclination of the binary system vs. the neutron star mass. For each point we also mark the mass of the companion star M_c (in units of $M_\odot$) and the mass ratio $q = M_c/M_{\rm NS}$.

only points where both the fundamental and the first overtone are detected with at least 3σ significance, we search for models that fit all observations (amplitude of fundamental and ratio of the first overtone to the fundamental) and which have the same mass and radius. Hot spot size and position are permitted to vary between observations since accretion flow is expected to be variable.

Although it is possible to obtain a high degree of harmonic content, due to general relativistic effects, from a single visible hot spot (see also Lamb et al. 2009), we find that the strength of the harmonic is such that two antipodal hot spots must be visible in order to fit the data. We are also able to constrain system geometry. The 1σ confidence contours restrict us to models with $\alpha \simeq 50^\circ$ and $\delta = (45\text{–}50)^\circ$; the 2σ contours permit a wider range of parameters but still require models where $\alpha = (40\text{–}50)^\circ$ and $\delta = (30\text{–}50)^\circ$ (hot spots must be smaller if they are located closer to the pole). These results, within the frame of our simple model, suggest a substantial offset between rotational and magnetic pole in this source.

Our models also put limits on stellar compactness. The 1σ confidence contours exclude models with $M/R > 0.17\,M_\odot\,{\rm km}^{-1}$, while the 2σ contours exclude models with $M/R > 0.18\,M_\odot\,{\rm km}^{-1}$. Although this does not rule out any common EoS (Lattimer & Prakash 2007), it does exclude some viable regions of dense matter parameter space.

Our simple calculations, while certainly not conclusive, illustrate the potential of this source. With better models and phase-resolved spectroscopy using high spectral resolution observations, this system is an extremely promising candidate for obtaining tight constraints from pulse-profile fitting.

We thank J. Poutanen for useful discussions. A.P. and M.L. acknowledge support from the Netherlands Organization for Scientific Research (NWO) Veni and Rubicon Fellowship, respectively.

REFERENCES

Altamirano, D., et al. 2010, ATel, 2565, 1
Beardmore, A. P., Godet, O., & Sakamoto, T. 2006, GRB Coordinates Network, 5209, 1
Belloni, T., et al. 2010, ATel, 2568, 1
Bozzo, E., et al. 2010, ATel, 2567, 1
Burrows, D. N., et al. 2005, Space Sci. Rev., 120, 165
Cadeau, C., et al. 2007, ApJ, 654, 458
Chakrabarty, D., Jonker, P. G., & Markwardt, C. B. 2010, ATel, 2585, 1
Chakrabarty, D., et al. 1993, ApJ, 403, L33
Chanan, G. A., Middleditch, J., & Nelson, J. E. 1976, ApJ, 208, 512
Chenevez, J., et al. 2010, ATel, 2561, 1
Eggleton, P. P. 1983, ApJ, 268, 368
Ferrigno, C., et al. 2011, A&A, in press (arXiv:1005.4554)
Gierliński, M., & Poutanen, J. 2005, MNRAS, 359, 1261
Hartman, J. M., et al. 2008, ApJ, 675, 1468
Hartman, J. M., et al. 2009, ApJ, 702, 1673
Ibragimov, A., & Poutanen, J. 2009, MNRAS, 400, 492
Jahoda, K., et al. 2006, ApJS, 163, 401
Lamb, F. K., et al. 2009, ApJ, 706, 417
Lattimer, J. M., & Prakash, M. 2007, Phys. Rep., 442, 109
Linares, M., van der Klis, M., & Wijnands, R. 2007, ApJ, 660, 595
Linares, M., et al. 2008, ApJ, 677, 515
Markwardt, C. B., & Strohmayer, T. E. 2010, ApJ, 717, L149
Markwardt, C. B., et al. 2010, ATel, 2576, 1
Nath, N. R., Strohmayer, T. E., & Swank, J. H. 2002, ApJ, 564, 353
Palmer, D., et al. 2006, GRB Coordinates Network, 5208, 1
Patruno, A. 2010, in Proc. Science: High Time Resolution Astrophysics IV—The Era of Extremely Large Telescopes—HTRA-IV, arXiv:1007.1108
Patruno, A., Wijnands, R., & van der Klis, M. 2009a, ApJ, 698, L60
Patruno, A., et al. 2009b, ApJ, 707, 1296
Patruno, A., et al. 2010, ApJ, 717, 1253
Pavan, L., et al. 2010, ATel, 2548, 1
Pechenick, K. R., Ftaclas, C., & Cohen, J. M. 1983, ApJ, 274, 846
Poutanen, J., & Gierliński, M. 2003, MNRAS, 343, 1301
Poutanen, J., Ibragimov, A., & Annala, M. 2009, ApJ, 706, L129
Schady, P., et al. 2006, GRB Coordinates Network, 5200, 1
Strohmayer, T. E., & Markwardt, C. B. 2010, ATel, 2569, 1
Wijnands, R., & van der Klis, M. 1998, Nature, 394, 344
Wijnands, R., et al. 2003, Nature, 424, 44
Wijnands, R., et al. 2009, MNRAS, 393, 126
Yang, Y. J., et al. 2010, ATel, 2579, 1